An assessment of Arctic Ocean freshwater content changes from the 1990s to the 2006 − 2008 period

Benjamin Rabe[a∗], Michael Karcher[a], Ursula Schauer[a], John M. Toole[b], Richard A. Krishfield[b], Sergey Pisarev[c], Frank Kauker[a∗], Rüdiger Gerdes[a], Takashi Kikuchi[d]

[a] Alfred Wegener Institute for Polar and Marine Research, Germany
[b] Woods Hole Oceanographic Institution, USA
[c] Shirshov Institute of Oceanology, Russia
[d] Japan Agency for Marine-Earth Science and Technology, Japan

December, 2010

Manuscript accepted for publication in Deep-Sea Research Part I

DOI: 10.1016/j.dsr.2010.12.002

*Corresponding author current address:
AWI for Polar and Marine Research
Bussestr. 24, Postfach 120161
27515 Bremerhaven, Germany
Ph: +49 (0)471 4831 2403
Fax: +49 471 4831 1797
email: Benjamin.Rabe@awi.de

Abstract

Unprecedented summer-season sampling of the Arctic Ocean during the period $2006-2008$ makes possible a quasi-synoptic estimate of liquid freshwater (LFW) inventories in the Arctic Ocean basins. In comparison to observations from $1992-1999$, LFW content relative to a salinity of 35 in the layer from the surface to the 34 isohaline increased by $8400 \pm 2000\ km^3$ in the Arctic Ocean (water depth greater than $500\,m$). This is close to the annual export of freshwater (liquid and solid) from the Arctic Ocean reported in the literature.

Observations and a model simulation show regional variations in LFW were both due to changes in the depth of the lower halocline, often forced by regional wind-induced Ekman pumping, and a mean freshening of the water column above this depth, associated with an increased net sea ice melt and advection of increased amounts of river water from the Siberian shelves. Over the whole Arctic Ocean, changes in the observed mean salinity above the 34 isohaline dominated estimated changes in LFW content; the contribution to LFW change by bounding isohaline depth changes was less than a quarter of the salinity contribution, and non-linear effects due to both factors were negligible.

Keywords: Arctic; Freshwater; Observation; Model; IPY; Upper Ocean

1 Introduction

Liquid freshwater (LFW) plays a major role in the Arctic Ocean: the vertical stratification in the halocline between the fresh surface layer and the salty, warm Atlantic Water (e.g. *Rudels et al.*, 2004) limits the upward transfer of heat and thus influences the formation and melting of sea ice (e.g. *MacDonald*, 2000). LFW affects not only the Arctic Ocean circulation but also influences the circulation in the Atlantic, as it is exported via the Fram Strait and the passages of the Canadian Arctic Archipelago into regions of deep water formation in the Nordic Seas and the North Atlantic (*Gerdes et al.*, 2008). Model studies have shown that this LFW export influences the large scale ocean circulation, such as the Meridional Overturning Circulation (MOC; e.g. *Koenigk et al.*, 2007; *Rennermalm et al.*, 2007) and the horizontal gyres (*Brauch and Gerdes*, 2005). LFW from the Arctic thus has a direct impact on climate (*Häkkinen*, 1999; *Haak et al.*, 2003)

The LFW budget of the Arctic Ocean (*Serreze et al.*, 2006; *Dickson et al.*, 2007) consists of inputs from Eurasian and North American river runoff, the Norwegian coastal current via the Eurasian shelves, precipitation, ice melt and the inflow from the Pacific through the Bering Strait; sinks of LFW are the export through the Canadian Arctic Archipelago and the western Fram Strait, and the formation and export of sea ice. Inflow of saline Atlantic Water (AW) occurs through the eastern Fram Strait and, in modified form, via the Barents Sea. The variability of this LFW budget, for instance the storage and export of LFW in the Arctic Ocean and the Nordic Seas (e.g. *Häkkinen and Proshutinsky*, 2004), is still not fully understood. From observations, (*Curry and Mauritzen*, 2005) found that $19000 \pm 5000\ km^3$ of freshwater [1] were added to the Nordic Seas and the Subpolar North Atlantic basins between the early 1965s and the 1995. Model studies have shown two strong negative anomalies in LFW export from the Arctic between 1970 and the mid 1990s. On average, the annual LFW export, referenced to a salinity of 35, was $500\ km^3$ higher between 1970 and 1995 than during the second half of the 20th century, when the time-mean export was $3050\ km^3/yr$ (*Köberle and Gerdes*, 2007; *Gerdes et al.*, 2008). The increased export represents a potential loss of LFW for the Arctic Ocean of $12500\ km^3$ between 1970 and 1995, close to the decline in the Arctic Ocean LFW reservoir in the model experiments during this time period and comparable to the LFW gain for the Nordic Seas and the Subpolar Basins described by *Curry and Mauritzen* (2005). Subsequent to 1995, the model

[1] they used the time average salinities from the 1950s in discrete layers as reference salinities to calculate the freshwater anomaly relative to that time period

studies show an accumulation of LFW in the Arctic Ocean and a decrease in LFW export up to 2001. On the other hand, an analysis of mooring based and ship based observations estimates the export of LFW from the Arctic Ocean through the western Fram Strait to be approximately constant between 1998 and 2008 (*de Steur et al.*, 2009).

During the 1990s the pathways of Pacific Water (PW) and Eurasian river water through the central Arctic changed relative to the prevailing conditions during the previous 40 years (*Steele et al.*, 2004; *Karcher et al.*, 2006; *Newton et al.*, 2008). Model studies indicate that the changes in the hydrography and circulation in the Arctic Ocean covary with large scale sea surface pressure and wind stress patterns (e.g. *Proshutinksy and Johnson*, 1997; *Dukhovskoy et al.*, 2004). *Proshutinsky et al.* (2009) analyzed observations in the Beaufort Gyre, which extends over the Beaufort Sea, the southern Canada Basin and often over parts of the Chukchi Plateau (CP; Figure 1). Their observations during July/August/September (JAS) from 1950 to 2007 show pronounced decadal variability and indicate a shift of the center of the gyre related to the large scale wind field. In an analysis based on the sparse observational data available over the past 100 years, *Polyakov et al.* (2008) infer a decrease in LFW in the Arctic Ocean from the mid-1960s to the mid-1990s. They attribute this to enhanced ice production and increased export of LFW driven by atmospheric circulation.

In this study, we analyze changes between two recent decades, making use of the unprecedented observational coverage during the International Polar Year ($2006 - 2008$) and observations over a longer time period during the 1990s. The data coverage allows us, for the first time, to use objective analysis to estimate not only the large scale spatial distribution of LFW and the LFW content but also quantify the error associated with these estimates. We focus on LFW calculated from salinity observations in the upper $500m$ of the whole deep Arctic Ocean bounded by the $500m$ isobath (Figure 1). Only observations during JAS are considered, as the year-round data coverage is strongly biased toward these months. The results will be put in context with other observations, underlying physical processes and output from a simulation with a coupled ice-ocean general circulation model, the North Atlantic/Arctic Ocean Sea Ice model (NAOSIM; *Karcher et al.*, 2003).

2 Methods

2.1 Observations

Salinity (S) profile data are taken from Conductivity Temperature Depth (CTD) and Expendable CTD (XCTD) observations from ships, submarines and ice drifting stations. Since 2004, these data have been augmented by autonomous measurements (*Kikuchi et al.*, 2007; *Krishfield et al.*, 2008), which, around the time of the International Polar Year (IPY; $2007-2009$), lead to an Arctic-wide coverage of measurements. The list of sources is given in Table 1. Despite the increasing number of observations from autonomous platforms there is a strong bias of data coverage toward Arctic summer. In order to avoid obscuring interannual variability with an unresolved seasonal cycle we use only data from JAS. Data used from the World Ocean Dataset 2009 (WOD09; *Boyer et al.*, 2009) are taken from the "CTD" part of the database ("High-resolution Conductivity-Temperature-Depth / XCTD data", as listed in the WOD09 documentation enclosed in the dataset). The accuracy of salinity observations is around 0.01 for XCTD after calibration with ship CTD profiles (*Itoh and Shimada*, 2003; *Kikuchi*, 2008) and the same for calibrated autonomous measurements. The manufacturer's stated accuracies for XCTD and Submerged Ship XCTD (SSXCTD) are 0.04 and 0.05, respectively. Where available, XCTD profiles that had been calibrated against conventional CTD profiles, reducing the error by a factor of two or more, were used. The accuracy of CTD casts from ships, calibrated against simultaneous water bottle samples, is generally an order of magnitude better than those of autonomous or expendable systems.

All observational data, also those taken from publicly accessible databases, were scrutinized to eliminate errors. Processing and quality control of the dataset are described in Appendix A and errors are discussed in Appendix B.

2.2 LFW calculations

To obtain a measure of LFW in the upper Arctic Ocean, the fraction of LFW content, f, relative to a reference salinity, S_{ref} (see also *Aagaard and Carmack*, 1989), was calculated between the surface and the depth of the 34 isohaline, $h = z(S = 34)$. This isohaline lies within the lower halocline, which has been shown to be largely unaltered by surface salinity throughout most of the Arctic Ocean

(*Rudels et al.*, 2004). The inventory of LFW in the layer above this isohaline is given by

$$h_{fw} = \int_{z=0\,m}^{h)} f\,dz = \int_{z=0\,m}^{h} \frac{S_{ref} - S}{S_{ref}}\,dz\ , \qquad (1)$$

where f is the fraction of LFW, S is the observed salinity and $S_{ref} = 35$, approximately the salinity of the AW inflow into the Arctic Ocean via the Fram Strait and the Barents Sea; using a reference salinity of 34.8 does not significantly change h_{fw} (see also Appendix B). River water, PW, net precipitation and ice melt are additions of LFW to the AW reference, whereas ice formation is a LFW sink. The maximum error in f due to accuracy of the salinity observations is about $2.5 \cdot 10^{-3}$. In cases where parts of the profile near the surface were not measured, the shallowest data point was used for constant extrapolation to the surface, making a mixed layer assumption. The maximum pressure of this data gap was set to $20\ dbar$, although most profiles have data from at least $8\ dbar$ (the potential error of this assumption is discussed in Appendix B).

Different subsets of the observations were objectively mapped to obtain the horizontal distribution of h_{fw} on a regular grid. The procedure is outlined in the following section. The mapped fields of h_{fw} for the whole deep Arctic Ocean bounded by the $500\ m$ isobath (Figure 1) were spatially integrated to obtain the LFW content between the ocean surface and h:

$$LFWC = \oint h_{fw}\,dA\ , \qquad (2)$$

where dA is the area associated with each grid point. h_{fw} and LFWC were calculated both from the observations and from output of the NAOSIM simulation.

2.3 Objective mapping

To obtain horizontal maps of h_{fw} for selected time periods, subsets of the observations were objectively mapped (e.g. *Bretherton et al.*, 1976) onto a uniform grid with $50\ km$ distance between grid points. Our procedure is similar to that used by *Böhme and Send* (2005) and *Böhme et al.* (2008). Following *McIntosh* (1990), the objective estimate of a parameter O at a grid point g can be obtained from a set of observations, O_d:

$$O_g =< O_d > +\omega \cdot (O_d- < O_d >) \; ; \; \omega = C_{dg} \cdot (C_{dd} + I\cdot < \eta^2 >)^{-1} \; , \tag{3}$$

where subscripts d and g refer to the observational (data) points and the grid points, respectively, $< O_d >$ is the mean of O_d, calculated as in *Owens and Wong* (2009) and *Bretherton et al.* (1976), ω is the weighting function and I is the identity matrix. The last term is the noise variance,

$$< \eta^2 >= \frac{\sum[n][i = 1](x_i - x_i c)^2}{2n} \; , \tag{4}$$

which is the mean of the squared deviation of each individual point in O_d (i) from it's nearest neighbor in O_d (ic), in terms of the mapping scales (e.g. *Holbrook and Bindoff*, 2000). This term measures the variations between close-by data, which is different to the signal variance that measures the squared deviation of the data from the mean. C_{dg} is the data-grid covariance and C_{dd} the data-data covariance. The interpolation (mapping) uses a Gaussian covariance function containing isotropic horizontal distance, D, and barotropic potential vorticity, PV (*Davis*, 1998):

$$PV = \frac{|\frac{f_d}{Z_d} - \frac{f_g}{Z_g}|}{\sqrt{\frac{f_d}{Z_d}^2 + \frac{f_g}{Z_g}^2}} \; ; \; D = |xy_d - xy_g| \; , \tag{5}$$

where xy is the geographic location, f the Coriolis parameter and Z the bathymetric depth, based on the International Bathymetric Chart of the Arctic Ocean (IBCAO, *Jakobsson et al.*, 2008). The covariance is given by

$$C =< s^2 > \; exp^{-(\frac{D^2}{L^2} + \frac{PV^2}{\Phi^2})} \; , \tag{6}$$

where the signal variance $< s^2 >= \frac{\sum_n^{i=1} (O_d - <O_d>)^2}{n}$, L represents the Gaussian decorrelation scale (e-folding scale) for D and Φ the scale for PV.

To avoid bias in the objective estimate, a reference field is often subtracted from the data before mapping. Therefore, we used Equation 4 in a two-stage procedure: First, a very smooth map of O_g was produced. Second, the residuals between each observed value and the mapped field were mapped using smaller spatial scales to give weight to the observations closest to each grid point. Finally, the mapped residuals were added to the mapped values from the first stage to obtain the horizontal map of

O_g. We separately mapped the observed h_{fw} and h. For the first stage mapping we used decorrelation scales of $L = 600\ km$ for horizontal distance and $\Phi = 1$ to adjust the isotropic distance scale to account for changes in barotropic potential vorticity, whereas the second stage used $L = 300\ km$, $\Phi = 0.4$. A distance of $300\ km$ has been shown to be the appropriate decorrelation scale for LFW observations in the Canada Basin (*Proshutinsky et al.*, 2009). Using $\Phi = 0.4$ for the non-isotropic potential vorticity scaling means that a depth change from around $3000\ m$ to $1500\ m$ at 85^o latitude sets the decay scale of the Gaussian covariance, i.e. typical bathymetric changes between deep Arctic basins and continental slopes or ridges. The combination of both the distance and potential vorticity scales leads to non-isotropic weighting contours around each grid point. For both mapping stages, only data within the large decorrelation scales from the grid point were used. If more than 60 data points were available, the data were subselected: $1/3$ were randomly chosen to avoid bias toward closely spaced profiles, such as from the Ice-Tethered Profilers (ITPs). The remaining $2/3$ were chosen by the highest weights (ω, Equation 4), where $1/3$ lied within the small decorrelation scale and $1/3$ within the large scale; note that at each grid point the covariance (and weighting) functions based on the large and the small scales do not necessarily have the same shape. Observations from JAS were mapped separately for the time periods $1992 - 1999$ and $2006 - 2008$.

To reduce errors in the maps of the LFW inventories, a gross range limit was used for all observed LFW inventories. Furthermore, regional outliers in the observed LFW inventories, as could be caused by eddies, were eliminated. For this purpose, each observed LFW inventory was compared to the mean of the inventories within a $600\ km$ radius. This mean and the standard deviation was calculated from all data or, if there were more than 60 data points, from a subset selected from within the $600\,km$ and a $100\ km$ radius in a similar way as during the mapping procedure. Each individual inventory was discarded if it was more than two standard deviations away from the mean or if the difference between the inventory and the mean was more than $7\ m$. A similar outlier elimination was applied to the depth of the 34 isohaline, h, prior to mapping. Finally, 858 profiles were used for the objective mapping for the time period $1992 - 1999$ and 4299 for $2006 - 2008$, the number for the latter period being greater mainly due to the frequent sampling of the autonomous CTD systems and increased observational efforts during the IPY.

A detailed analysis of the errors is given in Appendix B.

2.4 Numerical simulation

The numerical simulation was performed with the coupled ice-ocean model NAOSIM, which derives from the Geophysical Fluid Dynamics Laboratory modular ocean model MOM-2 (*Pacanowski*, 1995). The model domain contains the Arctic Ocean, the Nordic Seas and the Atlantic north of approximately 50^oN. Open boundary conditions in the Atlantic and in the Bering Strait were formulated following *Stevens* (1991), allowing the outflow of tracers and the radiation of waves. For the Bering Strait a net volume inflow of $0.8\ Sv$ has been applied. The initial and open boundary hydrography in January 1948 is taken from the PHC climatology (*Steele et al.*, 2001), which is also used as a reference for a surface salinity restoring with 180 days timescale. The model is driven with daily atmospheric forcing from 1948 to 2008 (NCEP/NCAR reanalysis, *Kalnay and coworkers*, 1996). For a more detailed description of the model see *Köberle and Gerdes* (2003) and *Kauker et al.* (2003). In an earlier model version NAOSIM has also been used to study freshwater dynamics of the Arctic Ocean (*Karcher et al.*, 2005; *Gerdes et al.*, 2008; *Rabe et al.*, 2009).

3 LFW distribution during $1992-1999$ and $2006-2008$

The observational maps show the maximum in the LFW inventories during JAS for both time periods in the Beaufort Sea (Figure 2). This maximum results from the persistent anticyclonic wind field, leading to Ekman pumping and a depression of the lower halocline in the Beaufort Gyre, and an accumulation of freshwater. There is a gradual decline in LFW from the Beaufort Sea toward the Siberian shelf seas and toward the Fram Strait and the Barents Sea, where AW enters the Arctic Ocean. Data coverage was overall good, except close to the Canadian Arctic Archipelago and in parts of the eastern Beaufort Sea during $1992-1999$ (Figure 2a). Time averages of the simulated LFW inventories show similar large scale distributions as the mapped observations for the corresponding time periods (Figure 3). However, the extrema in the Canada and Nansen basins are weaker in the simulation, in particular during $1992-1999$ (Figure 3a). Out of all the years under study, the simulation shows highest LFW inventories during 2008 (not shown).

A comparison of Δh_{fw} for the two periods (Figure 2c) exhibits an increase ranging from 1 to $8\,m$ of LFW in most of the deep Arctic Ocean except the western Nansen Basin, the eastern Amundsen Basin and part of the region north of the Canadian Arctic Archipelago. For the Beaufort Sea the changes hint at both a shift in the center of the Beaufort Gyre and an expansion of the gyre. In the central Arctic Ocean, *Steele and Boyd* (1998) observed a salinification in the central Arctic Ocean during the 1990s, resulting in a weakening of the stratification in the upper halocline. They attributed this to an eastward shift of the area influenced by fresh shelf waters. *Morison et al.* (2006) extended an analysis by *Steele et al.* (2004) up to 2005 to show that there is a 3 to 7 year lag in the adjustment of the upper Arctic Ocean to changes in the large scale wind field, represented by the Arctic Oscillation index. *Morison et al.* found that from 2000 onward, the observed hydrography of the central Arctic was again getting closer to the pre-1990s state. This was also shown by *Karcher et al.* (2005) in the same model simulation as used in our study. Our observations show that, regarding LFW, the trend continued up to the period 2006 to 2008.

A comparison of the LFW changes between the two time periods based on observations (Figure 2c) and the simulation (Figures 3c) shows strong similarities in the large scale pattern and amplitude. Regional differences are apparent, in particular in the Beaufort Sea and the southern Canada Basin, where the mapped observations show a shift in the LFW maximum toward the southeast; however, the lack of data north of the Canadian Arctic Archipelago during the 1990s prevents any conclusive comparison in this region. Over the whole deep Arctic Ocean, the observed LFWC (equation 2) increased by $8400\ km^3$ between the time periods $1992 - 1999$ and $2006 - 2008$. This is close to the estimated total annual export of freshwater (liquid and solid) from the Arctic Ocean (*Dickson et al.*, 2007) and almost $20\ \%$ of the average of LFWC we observe for both time periods. In the simulation, LFWC changed by $6120\ km^3$, which is lower than the observational estimate, but of the same order of magnitude. Nevertheless, in both the observations and the simulation we see changes in the distribution of LFW summing up to an overall increase in LFWC. In the following section we investigate possible causes of these changes.

4 Physical processes

4.1 LFW distribution

The LFW inventories are related to two quantities: the depth of the 34 isohaline, h, and the depth averaged salinity above this isohaline, $\bar{S}$. In most parts of the deep Arctic Ocean, the 34 isohaline is sufficiently deep, so that it is unaffected by wind-induced mixing and freezing-induced convection

(*Rudels et al.*, 2004). Therefore, the differences in h between $1992 - 1999$ and $2006 - 2008$ (Δh, Figure 4a) are likely to be the result of Ekman Pumping (EP) due to ocean surface stress induced by wind and ice motion (e.g. *Yang*, 2006). An exception to this is the region of the boundary current carrying AW from the Fram Strait and the Barents Sea. Here the 34 isohaline is very shallow, so that even small changes in the salinity of the AW inflow as well as changes in its temperature influencing ice formation and melt (e.g. *Schauer et al.*, 2004) have an effect on the depth of this isohaline. Unlike EP, which is an adiabatic process, changes in $\bar{S}$ ($\Delta\bar{S}$, Figure 4b) are diabatic (non-conservative), altered by changes in the salinity of advected water or local changes in sea ice melt and formation. We split the differences in h_{fw} between the two time periods into different components:

$$\Delta h_{fw} = \overbrace{\Delta h F_1}^{thickness} + \overbrace{h_1 \Delta F}^{salinity} + \overbrace{\Delta h \Delta F}^{non-linear}, \tag{7}$$

where $F_1 = 1 - \frac{\bar{S}_1}{S_{ref}}$, $\Delta F = -\frac{\Delta\bar{S}}{S_{ref}}$, and the subscript 1 denotes the reference values from $1992-1999$. The three terms on the right hand side will be referred to as labeled.

The 34 isohaline shallowed slightly in the central and eastern Canada Basin, i.e. the northeastern part of the Beaufort Gyre, and parts of the central Arctic (Figure 4a), whereas a distinct deepening can be seen around the Chukchi Plateau and in parts of the Makarov and Eurasian basins; deepening was less pronounced in the southeastern Beaufort Gyre. The effect on changes in the LFW inventories, given by the thickness term in Equation 7 (Figure 4c), is strongest around the Chukchi Plateau. The distribution of changes in h in the simulation (Figure 5a) shows good agreement with the observations on the large scale; in particular, north of the Bering Strait, both the simulation and the observations show an increase in h (Figures 5a and 4a), with a small east-west offset in the maximum. Different tendencies can be found north of Severnaya Zemlya in the Eurasian Basin and north of Greenland, where the mapped observations indicate a sinking of the halocline, while the simulation shows a rising.

For a calculation of surface stress induced EP, not only the wind stress but also the effect of internal ice stress has to be taken into account. Here, we make use of the ocean surface stress from the NAOSIM ice-ocean model simulation, which is forced with daily surface winds. The ocean surface stress comprises the joint effect of wind and internal ice stresses on the oceanic motion, and the EP calculation is based on this stress. Since even in regions of predominantly downward EP, such as the Beaufort Gyre, the 34 isohaline (or any other isohaline) is not displaced downward in the long term, its long-term average vertical velocity must be close to zero. The EP is counteracted by processes such as deep mixing that are not analyzed here in detail. Averaged regionally and in time over the whole 50 years of the simulation, the mean downward EP velocity is $0.5\,cm/day$ in the North American Basin and $1.5\ cm/day$ in the Beaufort Gyre. A comparison of the interannual variability in both regions, however, shows noticeable covariability between EP and the velocity associated with the displacement of the 34 isohaline (Figure 6). Only for a brief period in the 1990s, local mixing and externally driven lateral advection lead, on average, to stronger discrepancies between EP and the vertical velocity of the 34 isohaline. Thus, our model simulation supports earlier studies that EP is a key process for the determination of changes in h in the Beaufort Gyre (*Proshutinsky et al.*, 2009). In addition, our results indicate that this holds for the entire North American Basin.

In much of the deep Arctic Ocean we observe a decrease in $\bar{S}$ (Figure 4b) with values of $\Delta\bar{S}$ as low as -2 in the Makarov Basin and parts of the Eurasian Basin. Around the Chukchi Plateau and near the edges of the Eurasian Basin $\bar{S}$ increased. In the earlier period, h was lower in much of the Eurasian Basin than in the central Arctic and the Canada Basin. Therefore, the strong decreases in $\bar{S}$ in the Eurasian Basin lead to smaller increases in the LFW inventories due to the salinity term in Equation 7 (Figure 4d), than elsewhere. In the simulation the increases in $\bar{S}$ are similar to the observations north of the Bering Strait and north of the Fram Strait. The main simulated decrease is found in the Canada Basin, whereas there were weaker, localized decreases in the Eurasian Basin.

Changes in the net sea ice melt between the two time periods may have influenced $\bar{S}$ either locally or via advection of freshwater, (salt) from ice melt (formation), for example from the shelves. From the difference in simulated net sea ice melt between $2006-2008$ and $1992-1999$ (Figure 5c) we find a freshwater input from net melt around the Chukchi Plateau. This likely contributed to the decrease in salinity downstream to the east in the Beaufort Sea, evident in the maps of seen $\bar{S}$ from the observations (Figure 4b) and the simulation (Figure 5b). In much of the North American Basin, on the East Siberian and Laptev sea shelves and in the basins to the north net sea ice melt increased (Figure 5c), whereas in parts of the central Arctic and the Eurasian Basin small decreases occurred.

Although we observe an overall freshening in the Canada Basin, there was a redistribution of LFW in the southern part of the Beaufort Gyre (Figure 2c), associated with both changes in Δh (Figure 4a) and in $\bar{S}$ (Figure 4b). Here, tracer measurements between 1987 and 2007 show less removal of LFW within the surface layer due to a reduction in winter ice formation, whereas meteoric water (river runoff and precipitation) was increasing in the center of the gyre (*Yamamoto-Kawai et al.*, 2009); in 2006 and 2007, *Yamamoto-Kawai et al.* observed that also net ice melt increased in that part of the gyre. However, some of the observed increases in LFW near the surface were compensated by decreases in LFW contained in Pacific Water below (*Proshutinsky et al.*, 2009). Thus both a changed Ekman pumping due to changing ocean surface stress and an accumulation of river water and ice melt in the North American Basin have contributed to the observed changes between the two time periods.

In large parts of the Eurasian Basin, along the Lomonosov Ridge and in the Makarov Basin, we find that the observed increase in LFW can be mostly attributed to a decrease in the observed $\bar{S}$. Here, the simulation indicates no significant or uniform change in net sea ice melt (Figure 5c). Furthermore, there are indications from four years of hydrographic observations at the Lomonosov Ridge close to the North Pole since 1990 that ice melt water was not at an extreme high in 2007 (Bert Rudels pers. comm.). Tracer measurements (*Jones et al.*, 2008; *Anderson et al.*, 2004) and model simulations (*Karcher et al.*, 2006), on the other hand, suggest a change in the circulation of river water that was temporarily accumulating on the Siberian shelves and started to leave the shelves north of the East Siberian Sea around 1998. further east than previously. It subsequently replenished the 1990s LFW deficit in the central Arctic. This pulse of river water reached the Fram Strait in 2005, as observed by *Rabe et al.* (2009), and was also exported through the Canadian Arctic Archipelago. Observations have shown that the concentration of river water north of the Siberian Islands close to the Lomonosov Ridge was still higher in 2007 than in 1993 and 1995 (*Abrahamsen et al.*, 2009), suggesting that also in the central Arctic the observed increases in LFW between the two time periods studied in this paper were caused by high concentrations of river water.

In summary, observations and the NAOSIM simulation indicate that the components of the changes in LFW vary by region: the shift in the LFW maximum in the Beaufort Gyre is likely a consequence of a mixture of changes in net sea ice melt, wind-ice stress induced EP and accumulation of advected river water. Around the Lomonosov Ridge, the Makarov Basin and in the Eurasian Basin the increase in river water from the Siberian shelves made the strongest contribution, whereas changes in the layer depth, although large, contributed much less. In addition, changes in layer depth in the Eurasian Basin could not be associated with EP during the 1990s in the simulation. Therefore, the freshening in the Eurasian Basin between the two time periods must have been caused by the properties and distribution of inflowing water and changes in the formation of the lower halocline. The product of changes in h and $\bar{S}$, represented by the last term in Equation 7 (Figure 4e), played a role only in small parts of the

Eurasian Basin (Figures 4c and d).

4.2 LFW content

On average over the whole domain, i.e. the upper deep Arctic Ocean, the depth of the 34 isohaline increased by about $7\,m$ effecting a volume increase of about $31000\,km^3$, whereas the average salinity above this isohaline decreased by about 0.5. Nevertheless, the thickness term in Equation 7 gives an increase in LFWC by $1600\ km^3$, whereas the salinity term results in $+6500\ km^3$. This means that changes in $\bar{S}$ contributed much more to changes in LFWC than changes in h; therefore, EP primarily redistributed LFW within the Arctic Ocean. The fact that the integral of the thickness-term in Equation 7 over the whole deep Arctic Ocean is not zero may be explained by the regions where the 34 isohaline is not in the adiabatic interior or where the 34 isohaline reached onto the shelves. Furthermore, the thickness contribution is of the order of the uncertainty in the mapping process (Appendix 7). On the other hand, decreases in $\bar{S}$ originated from changes in ice formation and melt, and inflow of LFW from the shelves. The non-linear term gives an increase of less than $300\ km^3$ and is, therefore, negligible. Overall, the observed LFWC change is primarily due to changes in $\bar{S}$.

5 Summary and Conclusion

During July/August/September of $2006-2008$ salinity profiles were measured across all Arctic Ocean basins within a few years. These were used to analyze the distribution of LFW above the lower halocline represented by the 34 isohaline. The measurements from $2006 - 2008$ were compared to observations from the 1990s, where measurements were more sparse but still covered most of the deep Arctic Ocean.

1. The upper ocean LFW content for the deep Arctic Ocean during JAS increased by $8400 \pm 2000 km^3$ between $1992-1999$ and $2006-2008$. This is close to the annual export of freshwater (liquid and solid) to and from the Arctic Ocean and almost $20\ \%$ of the average LFW content observed for both time periods.

2. The spatial pattern of LFW changes simulated by NAOSIM agrees well with the observations

on large scales. The simulated LFW content change is, within the error margins, the same as what was derived from observations.

3. Over the whole domain, changes in the observed depth of the 34 isohaline lead to a redistribution of LFW and did not significantly influence the LFW content overall. In many regions, the changes in the depth of the 34 isohaline lead to changes in LFW; in particular, north of the Bering Strait, where the simulation suggests stronger anticyclonic stress during $2006 - 2008$, leading to a downward displacement of this isohaline due to downward Ekman pumping and hence to an increase in LFW. Only in regions where the lower halocline is formed, north of the Fram Strait and the Barents Sea, and north of the Canadian Arctic Archipelago, did we observe diabatic changes in the depth of the 34 isohaline.

4. The observed LFW changes were largely due to a freshening of the layer above the 34 isohaline. In the central Arctic, this was most likely due to enhanced advection of river water advected from the shelves. In certain regions, such as north of the Bering Strait, increases in LFW can be attributed to changes in the simulated net sea ice melt. In addition, the simulation shows increases in net sea ice melt on the Siberian shelves that may have been advected into the basins.

The observed change in the LFW content is equivalent to an average annual increase of about $750\ km^3$ between 1996 and 2007; the value in our simulation is about $550\ km^3$. These values are of similar magnitude as past changes seen in model studies by *Köberle and Gerdes* (2007) and *Gerdes et al.* (2008), where the LFW export from the Arctic Ocean between 1970 and 1995 was temporarily enhanced by $500 km^3$ annually, contributing to the LFWC decline in the Arctic over the same period. River runoff has not changed on an Arctic-wide scale (*Serreze et al.*, 2006). LFW transports through the Bering Strait have been shown to vary on an interannual to multi-year timescale, but no trend was observed between 1998 and 2008 (*Woodgate et al.*, 2006, and pers. comm.). *Dmitrenko et al.* (2008) have argued that, on average between 1920 and 2005, $500 km^3/yr$ of LFW were advected from the eastern Siberian shelf to the Arctic Ocean through the northeastern Laptev Sea during times of anticyclonic atmospheric circulation. This value is again of similar order as the changes we observed. Therefore, the most likely candidates for changing the LFWC between our two time periods are the LFW exports from the Arctic to the Nordic Seas and the North Atlantic and the exchange between the upper deep Arctic Ocean and the Siberian shelves.

Appendix

A Data processing procedures for salinity profiles

There are three categories of data we make use of in this study:

1. Data from ship CTDs directly obtained from the PIs only underwent a gross visual screening as these data were thoroughly processed and calibrated by the respective PIs and colleagues.

2. Data from WOD09 lying within our domain, the deep Arctic Ocean, only covers the first time period, $1992-1999$. All data with a WOD flag of 1 ("outside range") and 8 ("questionable data") were discarded (please refer to the WOD09 manual for a description of ranges by region and depth interval; *Boyer et al.*, 2009). Furthermore, the data were thoroughly screened for spikes, unrealistic gradients and noise in the salinity profiles as well as gross offsets in temperature-salinity space. Any erroneous data were discarded or were replaced with data of better quality, where available. For example, the SCICEX93 (Scientific Ice Expeditions, 1993) data in WOD09 is in almost raw format, but those data are also available in a more advanced stage of processing, where SSXCTD casts from the submarine under the ice were corrected using surface CTD casts from the same expedition (*Morison et al.*, 1998).

3. Autonomous ice-based profilers, the WHOI Ice-tethered Profiler (ITP) and the MetOcean Polar Ocean Profiling System (POPS) provided a large number of profiles for $2006-2008$. ITPs (*Krishfield et al.*, 2008) obtain profile data at about $0.25\,m$ vertical resolution ($1\,Hz$ CTD sampling rate). These data were corrected for CTD sensor lags (*Johnson et al.*, 2007) and screened for erroneous data. Subsequently, a conductivity correction was performed by comparing the lower part of the profile with objectively mapped independently measured salinity on selected isotherms (potential temperatures $\{0.3, 0.4, 0.5\}^oC$). After correction, the accuracy of the salinity data is 0.01. A detailed description of ITP processing procedures can be found in "ITP Data Processing Procedures" available at "http://www.whoi.edu/itp/data/". POPS (*Kikuchi et al.*, 2007) provide data only at discrete pressure intervals, ranging from $2\ dbar$ near the surface to $10\ dbar$ in the lower part of the profile. Hence, sensor correction could not be applied to the POPS data, but data were thoroughly screened for errors. Subsequently, a conductivity correction was performed, using historical data as a reference in a similar way as for the ITPs. The

POPS vertical resolution is still above that of ARGO profilers, which claim an accuracy of 0.01 in salinity, after conductivity correction against historical data (*Owens and Wong*, 2009, and references therein). Therefore, we assume this accuracy also holds for data from POPS.

Any profiles that did not meet the following criteria were discarded: data gaps ranging over more than $20\ dbar$ for either pressures lower than $150\ dbar$ or salinities less than 34.5; more than $30\ \%$ of the data missing in the layer above the 34 isohaline. The remaining profiles were interpolated onto $2\ dbar$ pressure levels, where interpolated values that were more than $3\ dbar$ away from any original data point were eliminated. This avoids implausible interpolation across strongly stratified parts of the water column. Some duplicate profiles were manually identified and removed from the combined dataset. Further duplicates were eliminated in cases where more than one profile was found with the same latitude, longitude, time stamp and maximum profile pressure, within the following margins: two decimal places for latitude / longitude, six hours for time and $50\ dbar$ for maximum profile pressure. Preference was given to profiles contained in datasets other than WOD09, if possible those obtained directly from the PIs responsible for their processing, as these data were of equal or better quality.

B Uncertainty in FWC estimates

The sources of error within our LFWC estimate consist of the statistical error associated with the mapping procedure, errors due to sampling gaps in regions of potentially high vertical gradients in salinity and errors due to the accuracy of the measurement devices.

The statistical mapping error is given at each grid point g by

$${\eta_g}^2 =< s^2 > -\omega \cdot C^T_{dg} + \frac{(1-\omega)^2}{\sum (C_{dd} + I \cdot < \eta^2 >)^{-1}}\,, \tag{8}$$

where the symbols are defined in Section 2.3.

We found η_g from mapping LFW to be highest ($> 1.5\ m$) in regions without data, such as north of the Canadian Arctic Archipelago, but significant errors ($\sim\ 1\ m$) were also found in regions of higher data coverage in the North American Basin due to uneven spatial distribution of the profiles and variability in the data (Figure 7). We tested the reliability of the LFWC estimate from the mapped

LFW inventories by considering only grid points below an error threshold: the difference in LFWC between $2006-2008$ and $1992-1999$ considering only grid points with $\eta_g < 1.5\ m$ is $8200\ km^3$, and using $\eta_g < 1\ m$ it is $7600\ km^3$; here, we use the field of combined error from both time periods, considering the higher error of the two at each grid point. Considering only $1992-1999$, the time period with the higher mapping error, the estimate of the error is $2000\ km^3$ using a threshold of $<\ 1.5\ m$, the same as that without a threshold, and $1800\ km^3$ using a threshold of $<\ 1\ m$. Hence, our estimate of the difference in LFWC based on mapped LFW inventories appears to be robust with respect to spatial coverage of the data. Furthermore, we performed the mapping with smaller distance scales, L, (potential vorticity scales, Φ, were unchanged) and compared the resulting map to the one in Figure 2c. Considering only grid points covered by both maps, we obtain a different LFWC for each comparison: First, using $100\ km$ and $50\ km$ as the large and small distance scales, respectively, lead to a difference in LFWC between both time periods of $5000\ km^3$. This compares to $5100\ km^3$ in the mapping with scales of 600 and $300\,km$. Second, mapping with $200/100\,km$ leads to $7700\,km^3$, which is the same as the value from the $600/300\ km$ map. The sensitivity of the LFWC difference between the two time periods due to the fraction of randomly chosen data points in the mapping process is around $100\ km^3$. using five independent mappings of the same data in each time period. Likewise, changing the reference salinity, S_{ref}, in Equation 1 to 34.8 only decreases the LFWC difference by $200\ km^3$. The sensitivity studies suggest that the difference in LFWC between both time periods is between 6000 and $10000\ km^3$

Data gaps in parts of the profile with strong vertical gradients of salinity near the surface may introduce additional error to the LFW inventories and thus the LFWC. For example, autonomous profilers, tethered to an ice floe, do not sample the top 7 to $10\ m$; some other salinity profiles are missing as much as the top $20\ m$, the maximum allowed in our selection. We tested potential errors in two ways:

1. A set of 215 CTD-based salinity profiles from two trans-Arctic Polarstern cruises, which took stations in all the four Arctic Basins, is used. The LFW inventories using the full profiles, usually starting at $2\ dbar$, are compared to inventories using the value from $10\ dbar$ in each profile as a constant to the surface. In all 215 profiles, the maximum difference between the salinity at $10\ dbar$ and the minimum salinity in the layer to the surface is 2, and only $12\ \%$ of these profiles show a salinity difference that leads to a difference in the LFW inventory of more than $0.05\,m$. This indicates that undersampling the upper $10\,dbar$ leads to an error smaller

than that given by the mapping procedure. One caveat of this comparison is that during CTD casts large research vessels evoke mixing of the upper 10 to $20\ m$ due to the use of strong stern or bow thrusters. While this does not affect vertically integrated quantities, such as our LFW inventories, it may not fully resolve shallow layers of ice melt.

2. The LFW inventories were calculated assuming that the data was missing in a pressure interval near the surface in all profiles. We did this calculation in two ways: First, we filled the artificial gap by making a mixed layer assumption, using the shallowest data point below the gap for constant extrapolation to the surface. Second, we did not fill the artificial gap, ignoring any data within the pressure interval. Assuming a mixed layer in the pressure interval 0 to $10\ dbar$ or 0 to $20\ dbar$, the resulting LFWC differences between the two time periods are $8000\ km^3$ or $6800\ km^3$, respectively. Even if we completely ignore the upper $10\ dbar$ or $20\ dbar$, we still obtain significant LFWC differences, $6700\ km^3$ or $4900\ km^3$, respectively. Regardless of how we treat any near-surface sampling gaps, the large scale patterns of the differences in LFW inventories between the two time periods are similar to the one in Figure 2c, which is why the corresponding maps are not shown here. Hence, the existence of near surface sampling gaps does not alter our conclusion that a significant increase in LFWC occurred between $1992-1999$ and $2006-2008$.

Acknowledgments

We thank the participants of the various observational efforts listed in Table 1 for obtaining and processing the salinity measurements. This work was supported by the Co-Operative Project “The North Atlantic as Part of the Earth System: From System Comprehension to Analysis of Regional Impacts” funded by the German Federal Ministry for Education and Research (BMBF) and by the European Union Sixth Framework Programme project DAMOCLES (Developing Arctic Modelling and Observing Capabilities for Long-term Environment Studies), contract number 018509GOCE. This work is a contribution to the ”Helmholtz Climate Initiative REKLIM” (Regional Climate Change), a joint research project by the Helmholtz Association of German research centres (HGF).

References

Aagaard, K., and E. C. Carmack (1989), The role of sea ice and other fresh water in the Arctic circulation, *J. Geophys. Res.*, *94*(C10), 14,485–14,498.

Abrahamsen, E. P., M. P. Meredith, K. K. Falkner, S. Torres-Valdes, M. J. Leng, M. B. Alkire, S. Bacon, S. W. Laxon, I. Polyakov, and V. Ivanov (2009), Tracerderived freshwater composition of the Siberian continental shelf and slope following the extreme Arctic summer of 2007, *Geophys. Res. Lett.*, *36*, L07602, doi:10.1029/2009GL037341.

Anderson, L. G., S. Jutterström, S. Kaltin, E. P. Jones, and G. Björk (2004), Variability in river runoff distribution in the Eurasian Basin of the Arctic Ocean, *J. Geophys. Res.*, *109*, doi:10.1029/2003JC001773.

Böhme, L., and U. Send (2005), Objective analyses of hydrographic data for referencing profiling float salinities in highly variable environments, *Deep-Sea Res. II*, *52*(3-4), 651–664, doi:10.1016/j.dsr2.2004.12.014.

Böhme, L., M. P. Meredith, S. E. Thorpe, M. Biuw, and M. Fedak (2008), The ACC frontal system in the South Atlantic: monitoring using merged Argo and animal-borne sensor data, *J. Geophys. Res.*, *113*, C09012, doi:10.1029/2007JC004647.

Boyer, T., J. I. Antonov, O. K. Baranova, H. E. Garcia, D. R. Johnson, R. A. Locarnini, A. V. Mishonov, T. D. O'Brien, D. Seidov, I. V. Smolyar, and M. M. Zweng (2009), World ocean database 2009, in *NOAA Atlas NESDIS*, vol. 66, edited by S. Levitus, U.S. Government Printing Office, Washington, D.C., 216 pp, DVDs.

Brauch, J. P., and R. Gerdes (2005), Reaction of the northern North Atlantic and Arctic oceans to a sudden change of the NAO, *J. Geophys. Res.*, *110*, C11018, doi:10.1029/2004JC002436.

Bretherton, F. P., R. E. Davis, and C. B. Fandry (1976), A technique for objective analysis and design of oceanographic experiments applied to MODE-73, *Deep-Sea Res. I*, *23*, 559582.

Curry, R., and C. Mauritzen (2005), Dilution of the Northern North Atlantic Ocean in Recent Decades, *Science*, *308*, 1772–1774, doi:10.1126/science.1109477.

Davis, R. E. (1998), Preliminary results from directly measuring middepth circulation in the tropical and South Pacific, *J. Geophys. Res.*, *103*(C11), 24,619–24,639.

de Steur, L., E. Hansen, R. Gerdes, E. Karcher, M. anFahrbach, and J. Holfort (2009), Freshwater fluxes in the East Greenland Current: A decade of observations, *Geophys. Res. Lett.*, *36*, L23611, doi:10.1029/2009GL041278.

Dickson, R., B. Rudels, S. Dye, M. Karcher, J. Meincke, and I. Yashayaev (2007), Current estimates of freshwater flux through Arctic and subarctic seas, *Progress in Oceanography*, *73*, 210–230, doi:10.1016/j.pocean.2006.12.003.

Dmitrenko, I. A., S. A. Kirillov, and L. B. Tremblay (2008), The long-term and interannual variability of summer fresh water storage over the eastern Siberian shelf: Implication for climatic change, *J. Geophys. Res.*, *113*, C03007, doi:10.1029/2007JC004304.

Dukhovskoy, D. S., M. A. Johnson, and A. Proshutinsky (2004), Arctic decadal variability: An auto-oscillatory system of heat and fresh water exchange, *Geophys. Res. Lett.*, *31*, L03302, doi:10.1029/2003GL019023.

Gerdes, R., M. Karcher, C. Köberle, and K. Fieg (2008), Simulating the long term variability of liquid freshwater export from the Arctic Ocean, in *Arctic-Subarctic Ocean Fluxes: Defining the role of the Northern Seas in climate*, edited by R. R. Dickson, J. Meincke, and P. Rhines, chap. 17, pp. 405–425, Springer Science and Business Media.

Haak, H., U. Jungclaus, U. Mikolajewicz, and M. Latif (2003), Formation and propagation of great salinity anomalies, *Geophys. Res. Lett.*, *30*, 1473, doi:10.1029/2003GL01765.

Häkkinen, S. (1999), A simulation of the thermohaline effects of a great salinity anomaly, *J. Climate*, *12*, 1781–1795.

Häkkinen, S., and A. Proshutinsky (2004), Freshwater content variability in the Arctic Ocean, *J. Geophys. Res.*, *109*, C03051, doi:10.1029/2003JC001940.

Holbrook, N. J., and N. L. Bindoff (2000), A statistically efficient mapping technique for four-dimensional ocean temperature data, *Journal of Atmospheric and Oceanic Technology*, *17*(6), 831846.

Itoh, M., and K. Shimada (2003), XCTD salinity calibration in the Arctic Ocean, *Tech. Rep. 48*, Report of Japan Marine Science and Technology Center (JAMSTEC-R), JAMSTEC, Yokosuka, Japan.

Jakobsson, M., R. Macnab, M. Mayer, R. Anderson, J. Edwards, M.and Hatzky, H.-W. Schenke, and P. Johnson (2008), An improved bathymetric portrayal of the Arctic Ocean: Implications for ocean modeling and geological, geophysical and oceanographic analyses, *Geophys. Res. Lett.*, *35*, doi:10.1029/2008GL033520.

Johnson, G. C., J. M. Toole, and N. G. Lason (2007), Sensor Corrections for Sea-Bird SBE-41CP and SBE-41 CTDs, *J. Atmos. Ocean. Technol.*, *24*(6), 1117–1130, doi:DOI:10.1175/JTECH2016.1.

Jones, E. P., L. G. Anderson, S. Jutterström, L. Mintrop, and J. H. Swift (2008), Pacific fresh water, river water and sea ice meltwater across Arctic Ocean basins: Results from the 2005 Beringia Expedition, *J. Geophys. Res.*, *113*, C08012, doi:10.1029/2007JC004124.

Kalnay, E., and coworkers (1996), The NCEP/NCAR 40-Year Reanalysis Project, *Bull. Am. Meteorol. Soc.*, *77*(3), 437–495.

Karcher, M., R. Gerdes, F. Kauker, C. Köberle, and I. Yashayaev (2005), Arctic Ocean change heralds North Atlantic freshening, *Geophys. Res. Lett.*, *32*, doi:10.1029/2005GL023861.

Karcher, M., R. Gerdes, and F. Kauker (2006), Modeling of δ_{18}O and $_{99}$Tc dispersion in Arctic and subarctic seas, *ASOF Newsletter*, *5*, available from: <http://asof.npolar.no>.

Karcher, M. J., R. Gerdes, F. Kauker, and C. Köberle (2003), Arctic warming: Evolution and spreading of the 1990s warm event in the Nordic seas and the Arctic Ocean, *J. Geophys. Res.*, *108*(C2), doi:doi10.1029/2001JC001265.

Kauker, F., R. Gerdes, M. Karcher, C. Köberle, and J. L. Lieser (2003), Variability of Arctic and North Atlantic sea ice: A combined analysis of model results and observations from 1978 to 2001, *J. Geophys. Res.*, *108*(C6), doi:doi10.1029/2002JC001573.

Kikuchi, T. (2008), XCTD observation, in *The Expedition ARKTIS-XXII/2 of the Research Vessel "Polarstern" in 2007*, *Reports on polar and marine research*, vol. 579, edited by U. Schauer, pp. 96–102, Alfred-Wegener Institute for Polar and Marine Research: Bremerhaven, Germany.

Kikuchi, T., J. Inoue, and D. Langevin (2007), Argo-type profiling float observations under the Arctic multiyear ice, *Deep-Sea Res. I*, *54*(9), 1675–1686.

Köberle, C., and R. Gerdes (2003), Mechanisms determining the variability of Arctic sea ice conditions and export, *J. Climate*, *16*, 2843–2858.

Köberle, C., and R. Gerdes (2007), Simulated variability of the Arctic Ocean fresh water balance 1948-2001, *J. Phys. Oceanogr.*, *37*, 1628–1644, doi:10.1175/JPO03063.1.

Koenigk, T., U. Mikolajewicz, H. Haak, and J. Jungclaus (2007), Arctic freshwater export in the 20th and 21st centuries, *J. Geophys. Res.*, *112*, G04S41, doi:10.1029/2006JG000274.

Krishfield, R., J. Toole, A. Proshutinsky, and M. L. Timmermans (2008), Automated Ice-Tethered Profilers for seawater observations under pack ice in all seasons, *J. Atmos. Oceanic Tehnol.*, *25*, 2091–2105.

MacDonald, R. W. (2000), Arctic estuaries and ice: a positive-negative estuarine couple, in *The freshwater budget of the Arctic Ocean*, *NATO Science Partnership Sub-Series: 2*, vol. 70, edited by

E. L. Lewis, E. P. Jones, P. Lemke, T. D. Prowse, and P. Wadhams, pp. 383–407, Kluwer Academic: Netherlands.

McIntosh, P. C. (1990), Oceanographic data interpolation: objective analysis and splines, *J. Geophys. Res.*, *95*(C8), 13,529.

Morison, J., M. Steele, T. Kikuchi, K. Falkner, and W. Smethie (2006), Relaxation of central Arctic Ocean hydrography to pre-1990s climatology, *Geophys. Res. Lett.*, *33*, L17604, doi: 10.1029/2006GL026826.

Morison, J. H., M. Steele, and R. Andersen (1998), Hydrography of the upper Arctic Ocean measured from the nuclear submarine USS Pargo, *Deep-Sea Res. I*, *45*, 15–38.

Newton, R., P. Schlosser, D. G. Martinson, and W. Maslowski (2008), Freshwater distribution in the Arctic Ocean: simulation with a high resolution model and model-data comparison, *J. Geophys. Res.*, *113*, C05024, doi:10.1029/2007JC004111.

Owens, W. B., and A. Wong (2009), An improved calibration method for the drift of the conductivity sensor on autonomous CTD profiling floats by -S climatology, *Deep-Sea Res. I*, *56*(3), 450.

Pacanowski, R. C. (1995), MOM 2 Documentation, users guide and reference manual, *GFDL Ocean Group Tech. Rep. 3*, Geophys. Fluid Dyn. Lab., Princeton Univ., Princeton, N. J.

Polyakov, I. V., V. Alexeev, F. I. Belchansky, I. A. Dmitrenko, V. Ivanov, S. Kirillov, A. Korablev, M. Steele, L. A. Timokhov, and I. Yashayaev (2008), Arctic Ocean freshwater changes over the past 100 year and their causes, *J. Climate*, *21*(2).

Proshutinksy, A. Y., and M. A. Johnson (1997), Two circulation regimes of the wind-driven Arctic Ocean, *J. Geophys. Res.*, *102*, 12,493–12,514.

Proshutinsky, A., R. Krishfield, M.-L. Timmermans, J. Toole, E. Carmack, F. McLaughlin, W. J. Williams, S. Zimmermann, M. Itoh, and K. Shimada (2009), Beaufort Gyre freshwater reservoir: State and variability from observation, *J. Geophys. Res.*, *114*, doi:10.1029/2008JC005104.

Rabe, B., A. Mackensen, U. Schauer, M. Karcher, E. Hansen, and A. Beszczynska-Möller (2009), Freshwater components and transports in the FRAM Strait: Recent observations and changes since the late 1990s, *Ocean Sci.*, *5*, 219–233, doi:10.5194/os-5-219-2009.

Rennermalm, A. K., E. F. Wood, A. J. Weaver, M. Eby, and S. J. Derý (2007), Relative sensitivity of the Atlantic meridional overturning circulation to river discharge into Hudson Bay and the Arctic Ocean, *J. Geophys. Res.*, *112*, G04S45, doi:10.1029/2006JG000330.

Rudels, R., E. P. Jones, U. Schauer, and P. Ericksson (2004), Atlantic sources of the Arctic Ocean surface and halocline waters, *Polar Research*, *23*(2), 181–208.

Schauer, U., E. Fahrbach, S. Østerhus, and G. Rohardt (2004), Arctic warming through the Fram Strait: Oceanic heat transport from 3 years of measurements, *J. Geophys. Res.*, *109*, doi:10.1029/2003JC001823.

Serreze, M. C., a. P. Barrett, A. G. Slater, R. Woodgate, K. Aagaard, R. B. Lammers, M. Steele, R. Moritz, M. Meredith, and C. M. Less (2006), The large-scale freshwater cycle of the Arctic, *J. Geophys. Res.*, *111*(C11), doi:10.1029/2005JC003424.

Steele, M., and T. Boyd (1998), Retreat of the cold halocline layer in the Arctic Ocean, *J. Geophys. Res.*, *103*(C5), 10,419–10,439.

Steele, M., R. Morley, and W. Ermold (2001), PHC: A global ocean hydrography with a high quality Arctic Ocean, *J. Climate*, *14*, 2079–2087.

Steele, M., J. Morison, W. Ermold, I. Rigor, M. Ortmeyer, and K. Shimada (2004), Circulation of summer Pacific halocline water in the Arctic Ocean, *J. Geophys. Res.*, *109*, doi:doi10.1029/2003JC002009.

Stevens, D. P. (1991), On open boundary condition in the United Kingdom 979 Fine-Resolution Antarctic Model, *J. Phys. Oceanogr.*, *21*, 1494–1499.

Woodgate, R. A., K. Aagaard, and T. J. Weingartner (2006), Interannual changes in the Bering Strait fluxes of volume, heat and freshwater between 1991 and 2004, *Geophys. Res. Lett.*, *33*, doi:10.1029/2006GL026931.

Yamamoto-Kawai, M., F. A. McLaughlin, E. C. Carmack, S. Nishino, K. Shimada, and N. Kurita (2009), Surface freshening of the Canada Basin, 2003-2007: River runoff versus sea ice meltwater, *J. Geophys. Res.*, *114*, C00A05, doi:10.1029/2008JC005000.

Yang, J. (2006), The seasonal variability of the Arctic Ocean Ekman transport and its role in the mixed layer heat and salt fluxes, *J. Climate*, *19*, 5366–5387.

Tables and figures

Expedition, project or institute	Year(s)	Platform	Source URL or contact
World Ocean Database 2009	1992 – 1999	various	http://www.nodc.noaa.gov/OC5/WOD09
Scientific Ice Exercises (SCICEX)	1993	US submarines	http://data.eol.ucar.edu/codiac/dss/id=106.arcss072/
ARK IX/4	1993	RV Polarstern	http://www.pangaea.de/
ARK XI	1995	RV Polarstern	http://www.pangaea.de/
ARK XII	1996	RV Polarstern	http://www.pangaea.de/
Scientific Ice Exercises (SCICEX)	1996, 1997 and 1998,	US submarines	SAIC project, Sergey Pisarev (pisarev@ocean.ru)
ARK XIII	1997	RV Polarstern	http://www.pangaea.de/
Scientific Ice Exercises (SCICEX)	1997 and 1998,	US submarines	http://data.eol.ucar.edu/codiac/dss/id=106.arcss064/
ARK XV	1999	RV Polarstern	http://www.pangaea.de/
Beaufort Gyre Project	2006 – 2008	various ships	http://www.whoi.edu/beaufortgyre/
European Union project DAMOCLES	2006 – 2008	POPS	http://www.ipev.fr/damocles/
ARGO	2006 – 2008	POPS	http://www.coriolis.eu.org/cdc/argo.htm
Woods Hole Oceanographic Institution (WHOI)	2006 – 2008	ITP	http://www.whoi.edu/itp
ARK XXII/2 (SPACE)	2007	RV Polarstern	http://www.pangaea.de/
LOMROG 2007	2007	RV Oden	Göran Björk (gobj@gvc.gu.se)
Nansen / Amundsen Basins Observ. System (NABOS)	2007, 2008	various ships	http://nabos.iarc.uaf.edu/
ARK XXIII/3 (AMEX I)	2008	RV Polarstern	http://www.pangaea.de/
Arctic Summer Cloud Ocean Study (ASCOS)	2008	RV Oden	http://www.ascos.se (Anders Sirevaag)

Table 1: Data sources for salinity observations during JAS. The autonomous measurements were undertaken using the Ice-Tethered Profiler (ITP) and the Polar Ocean Profiling System (POPS). Data taken from the online World Ocean Database 2009 (WOD09; *Boyer et al.*, 2009) were used to augment but not replace profiles from the other datasets listed in the table. SCICEX data from the SAIC project were used, where available, to replace profiles from the 1997 and 1998 SCICEX expeditions downloadable from EOL. The SCICEX 1993 data from EOL were preferred over those from SAIC due to more advanced processing.

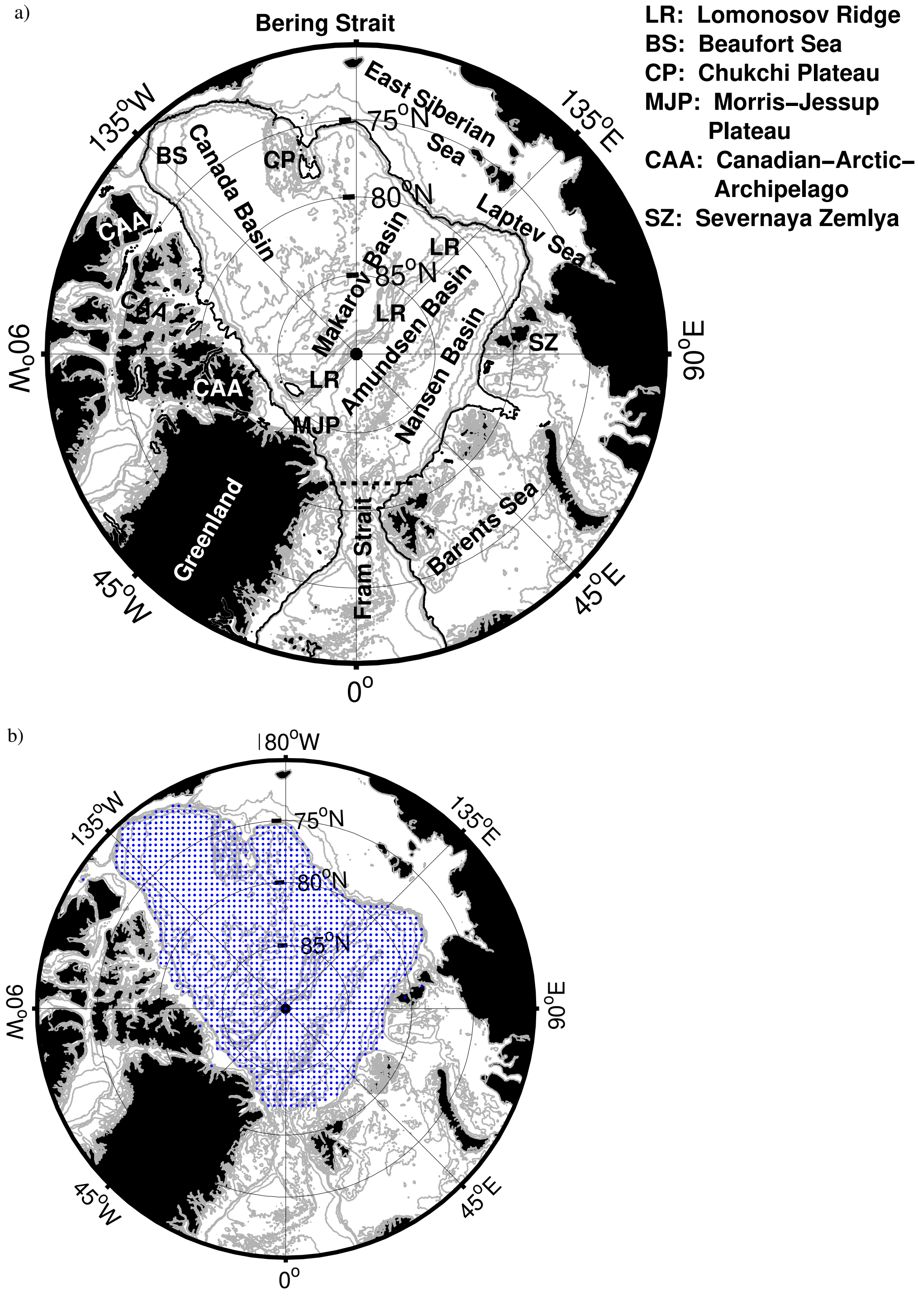

Figure 1: Bathymetry of the Arctic Ocean from the IBCAO database (IBCAO *Jakobsson et al.*, 2008): (a) geographic names; gray contour lines represent the bathymetric depths 100, 200, 500, 750, 1000, 2000, 3000 and 4000 m. The 500 m isobath represents the boundary of our "deep Arctic Ocean" domain and is shown as a thick black line; additionally, the domain was restricted to north of $82^o N$ north of the Fram Strait (dashed line). Whenever we refer to the "North American Basin" and the "Eurasian Basin" it incorporates the Makarov and Canada basins and the Amundsen and Nansen basins, respectively. (b) Grid used for objective mapping.

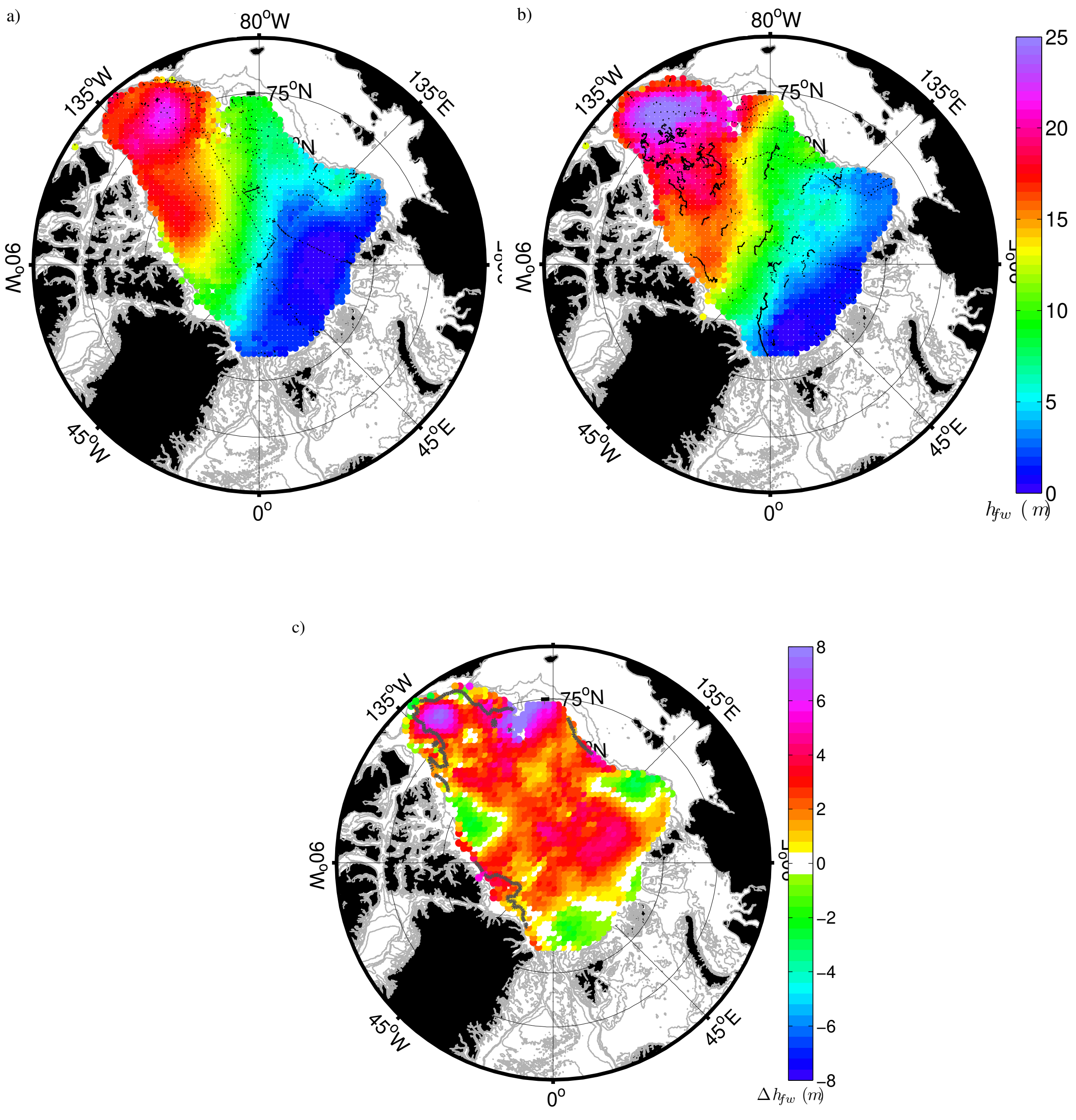

Figure 2: Objectively mapped observed freshwater inventory from the surface to the depth of the 34 isohaline for the deep Arctic Ocean during JAS: (a) $1992 - 1999$ and (b) $2006 - 2008$. The anomaly of $2006 - 2008$ relative to $1992 - 1999$ is shown in (c). The locations of measured salinity profiles used for the mapping are shown as black dots in (a) and (b); larger dots are shown in Figure 7. Only (c): values within $\pm 0.25\ m$ of zero are white; the thick gray line represent the $1\ m$ contour of the combined (maximum) statistical error estimate for both mapping time periods (see Figure 7).

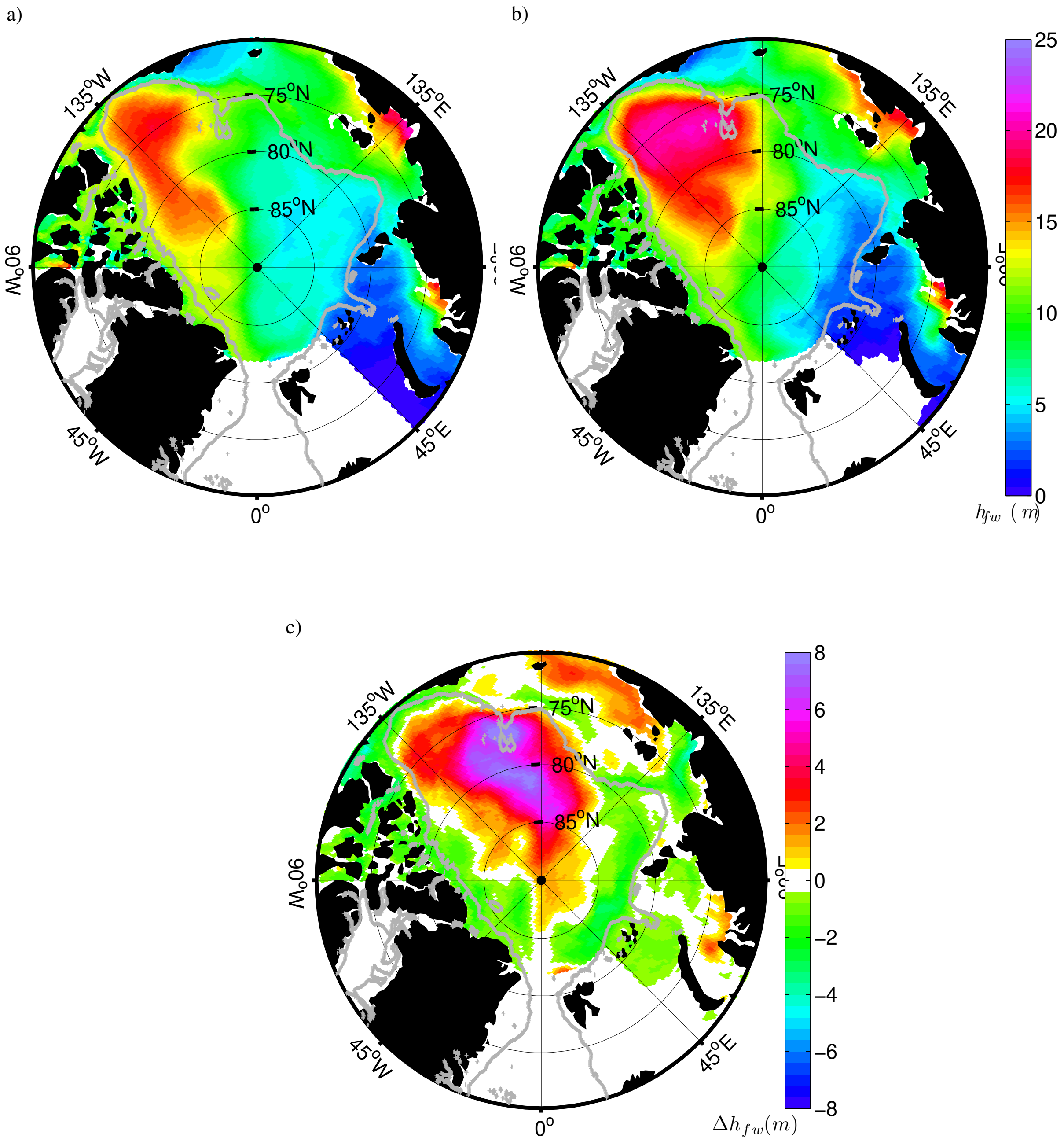

Figure 3: Time averages of freshwater inventories from the surface to the depth of the 34 isohaline in the NAOSIM simulation during JAS for the time periods (a) $1992-1999$ and (b) $2006-2008$, and (c) the anomaly of $2006-2008$ relative to $1992-1999$. The thick gray line represents the $500\ m$ isobath (IBCAO bathymetry), and the region south of 82^oN in the Fram Strait is left blank, as it is not considered in the analysis.

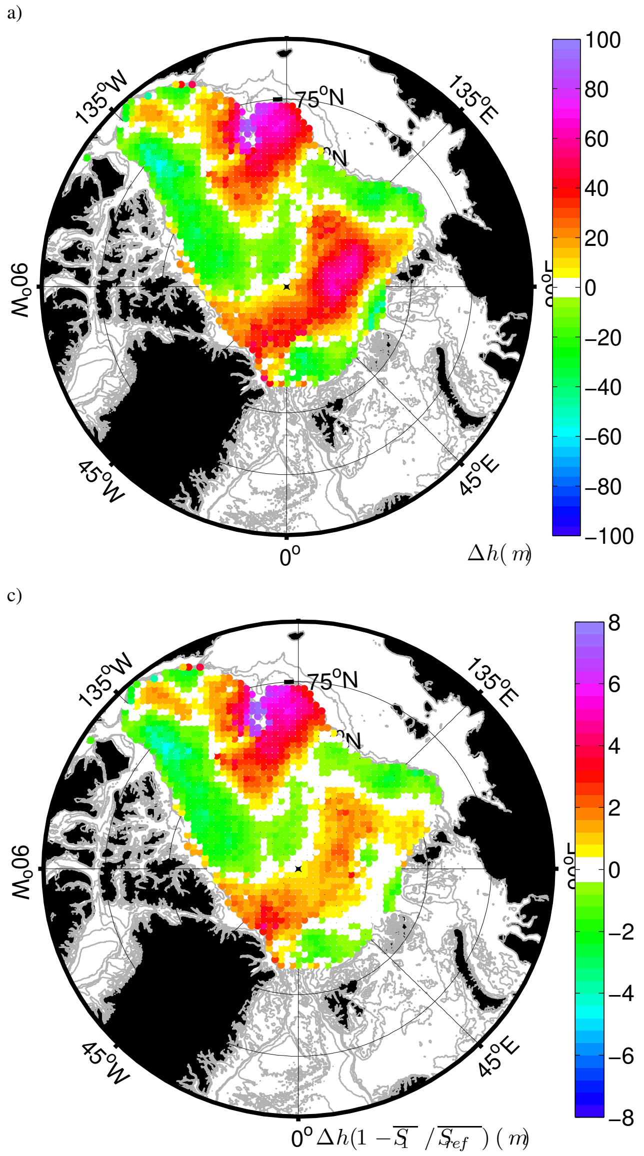

Figure 4: Difference between $2006-2008$ and $1992-1999$ from observations in the deep Arctic Ocean during JAS of (a) the depth of the 34 isohaline, $h = z(S = 34)$, and (b) the mean salinity above the 34 isohaline. (c), (d) and (e) show the "thickness", "salinity" and "non-linear" terms in Equation 7, respectively. Values within $\pm 0.25\ m$ (a and c to e) or ± 0.125 (b) of zero are white.

e)

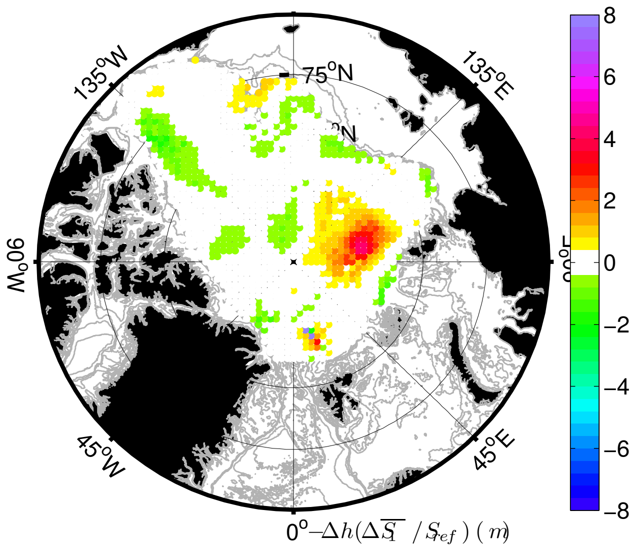

Figure 4: continued...

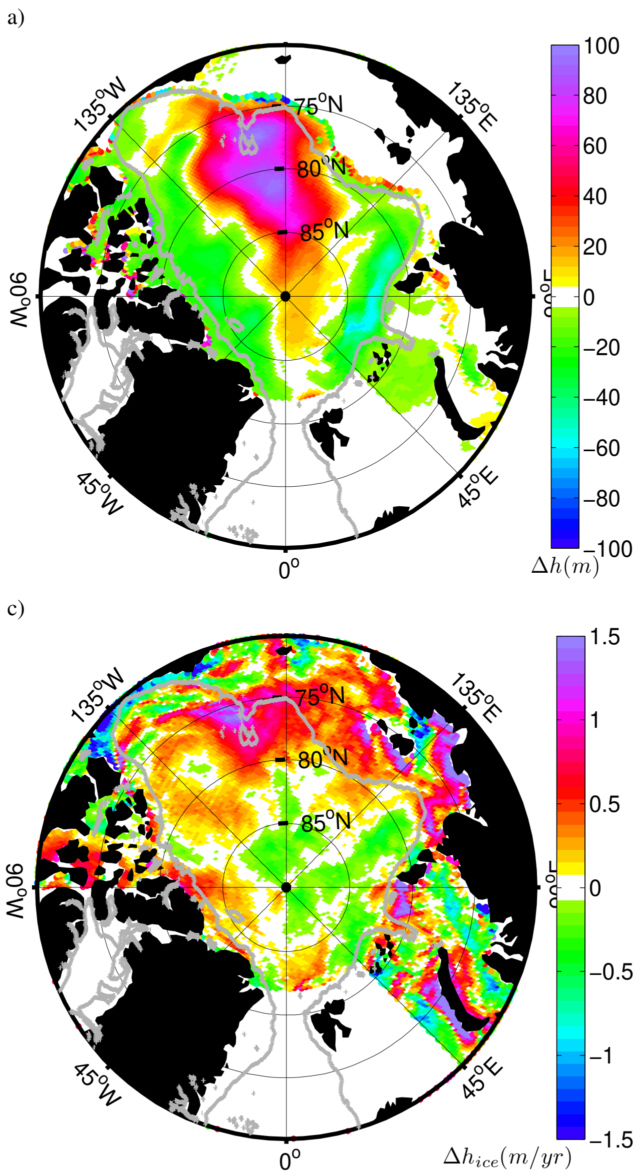

Figure 5: Difference in time averages from the NAOSIM simulation between the time periods $2006-2008$ and $1992-1999$: (a) depth of the 34 isohaline (JAS), (b) depth-averaged salinity above this isohaline (JAS), and (c) the net sea ice melt (all year). Positive values in (d) represent a reduction in thermodynamic sea ice growth or an increase in sea ice melt. The $500\,m$ isobath (IBCAO bathymetry) is shown as a thick gray line, and the region south of $82^o N$ in the Fram Strait is left blank, as it is not considered in the analysis.

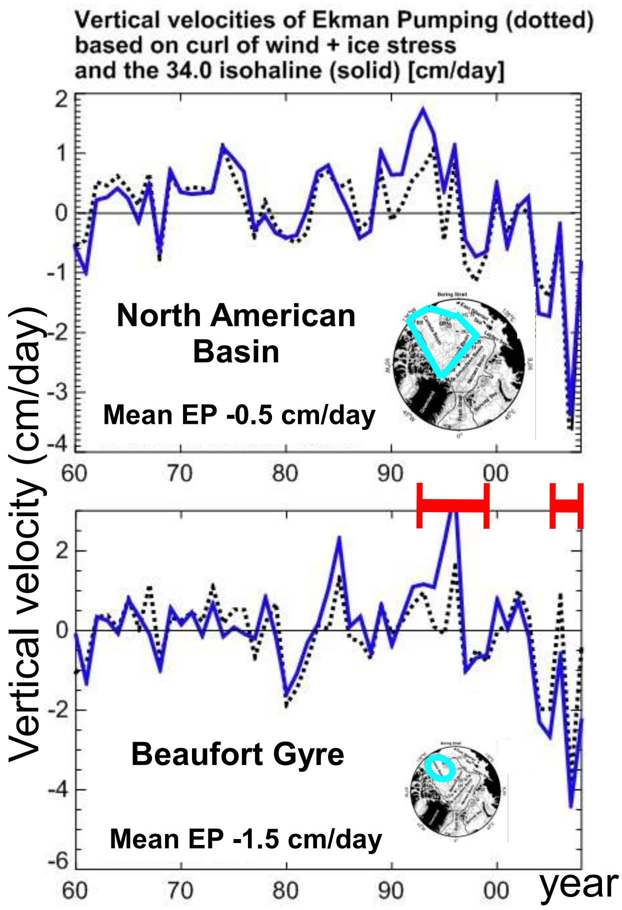

Figure 6: Time series of annual mean vertical velocity (positive upward) in the NAOSIM simulation derived from Ekman Pumping (EP; dotted), based on the curl of the ocean-surface (wind and ice) stress, and from the vertical displacement of the 34.0 isohaline (solid). Shown is the spatial means for the North American Basin and the Beaufort Gyre, where the EP velocity is offset by the time mean for each region. The regions used for spatial averaging are sketched in the inlaid maps, and the x-axis shows the time from 1960 until 2008 (middle-of-year), where the two time periods under study in our FW analysis are marked as red horizontal bars.

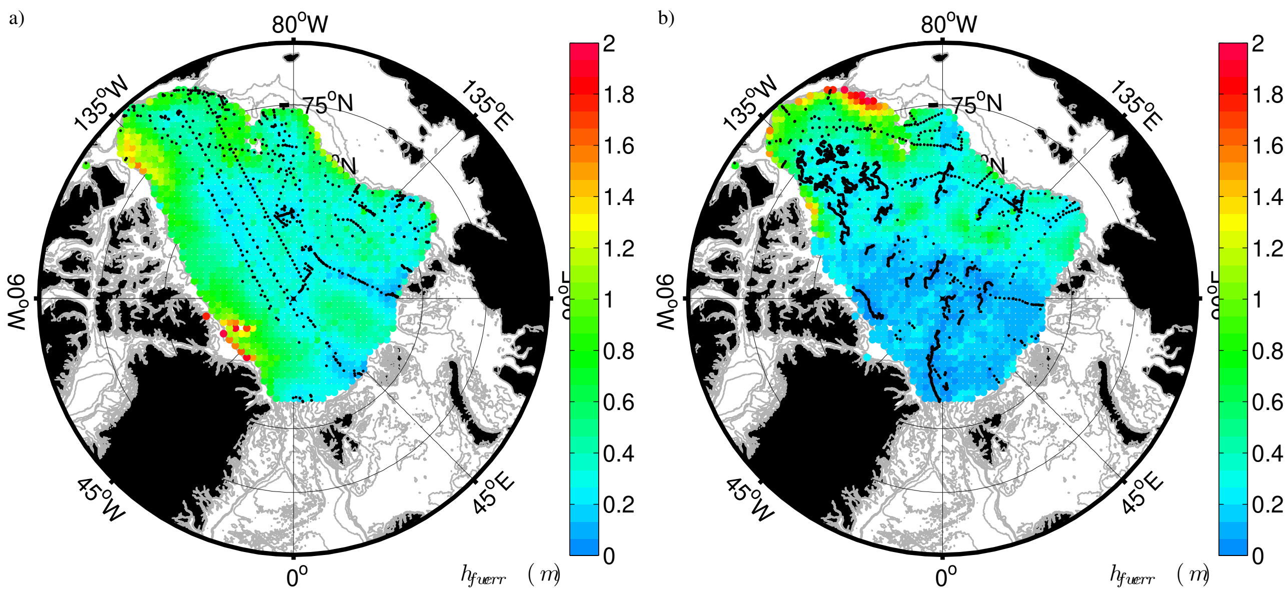

Figure 7: Statistical error estimate (Equation 8) associated with the objective maps of freshwater inventories in Figure 2: (a) $1992-1999$ and (b) $2006-2008$. The locations of measured salinity profiles used for the mapping are shown as black dots.